Investigation of Key Cellular Targets in Atrial Fibrillation Induced Electromechanical Remodeling using Human Atrial Cardiomyocytes Model

Fazeelat Mazhar[1], Chiara Bartolucci[1], Cristiana Corsi[1], Stefano Severi[1]

[1]University of Bologna, Cesena, Italy

Abstract

Atrial Fibrillation (AF) is the most common arrhythmia with a complex pathophysiology. In experiments, it becomes quite challenging to dissect the key mechanisms behind the AF induced remodeling effect. Using the power of computational modeling, we have developed a chronic atrial fibrillation version of our recently developed human atrial electromechanical cardiomyocyte model. Using an incremental approach, the model incorporates the remodeling effect in parameters related to electrical/ionic currents, Ca^{2+}-handling, the myofilament and the CaMKII effect. Based on this model, we have identified that at basal rate AF induced raised diastolic Ca-transient level is due to loss of SERCA function. Similarly, reduced cross-bridge cycling rate also contributes to elevated level of diastolic phase of contractility. Using this model, we extended the simulation for higher rates, and we found that under chronic AF (cAF) condition, the biphasic trend of contractility with rate was lost. Though the percentage change in Ca^{2+} and force was large due to raised diastolic levels. Thus, the model is a useful tool for future understanding cellular level mechanisms of other arrhythmias.

1. Introduction

Atrial Fibrillation (AF) remains a major clinical problem because of its impact on morbidity and mortality of millions of people [1]. The progressive nature of the disease eventually leads to a persistent (chronic) form of AF (cAF) that last for more than a year. Over the past 20 years, knowledge about the cellular and molecular targets of the AF induced remodelling has been enhanced [2]. However, the complex pathophysiology of the AF supported by a multitude of regulatory feedbacks makes it challenging to dissect the proarrhythmic phenotypes experimentally [2]. Therefore, for the translation of AF remodelling targets to the effective therapeutic prevention, we need to clearly understand each underlying mechanism.

Computational modeling is a powerful tool that provides complete control of parameters along with the visibility of all the individual components of the integrated system [3]. Recently, we have developed an electromechanically (EM) coupled model with proper consideration of feedforward and feedback pathways [4]. The model incorporates detailed Ca^{2+}-handling formulation and hence, demonstrates the time dependent heterogenous rise of Ca^{2+} in the cytosol. Using this model, we have proposed a cAF version by incorporating AF induced remodeling effect. We analysed the model characteristics at basal rate and later extended it for higher rates. Under cAF, we found a 79% depression in contraction with elevated diastolic level than control. Overall, the model has the potential to analyse the underlying mechanisms behind the physiological and pathological conditions and therefore, will be beneficial for future EM coupled studies.

2. Methods

Table 1: Atrial Fibrillation induced remodeling effect on model parameters.

Remodeling	Parameters modified	Reference
Electrical	g_{Na} ↓ 10%, g_{CaL} ↓ 50%, g_{to} ↓ 80%, g_{Kur} ↓ 55%, g_{Ks} ↑ 2-folds, and g_{K1} ↑ 2-folds. k_{NaCa} ↑ 40%, RyR gates sensitivity ↑ 50%, and Ca-SR leak ↑ 25%.	[5, 6]
CaMKII	expression ↑ 40%, activation ↑ 50%	[7, 8]
MCF	k_{off} ↓ 30%, k_d ↓ 50%, γ ↓ 30%	manual tunning
SERCA	pumping rate ↓ 20%, sensitivity ↑ 15%.	

We have developed a cAF version of our recently developed EM coupled human atrial cardiomyocyte model i.e., MBS2022 [4]. Briefly, the model has a two compartmental setup for cytosol i.e., the sub-space (*ss*) and the bulk cytosol (*bc*) with a contractile machinery operated by troponin (TRPN) buffer. Apart from this, the SR is also localized near the center, and it contains two compartments as cytosol SR_{ss} and SR_{bc} with their own release (RyR) and

uptake (SERCA) units. The rise in Ca^{2+} level in the bulk binds to TRPN and initiates the contraction; then unbinds back to its diastolic level. Hence, the MBS2022 model is a simplified EM model and is capable to simulate both mechano-electric (MEF) (AP by I_{sac}) and mechano-calcium (MCF) (Ca^{2+}-TRPN binding) feedback effects quantitatively.

To incorporate the cAF-induced remodeling effect in the model at the basal rate (BCL=1sec) we adopted an incremental approach. The first step was to include the electrical remodeling effect induced by the adaptation of both ionic and Ca^{2+}-handling machinery [5, 6] as shown in Table 1. The second step was to incorporate the AF induced increased CaMKII phosphorylation effect as was found in experiments [7, 8] and was remodeled as shown in Table 1. For activation, we increased the CaMKII binding rate, i.e. α_{CaMKII} and reduced the unbinding rate i.e. β_{CaMKII}.

Following the incremental approach, we included the myofilament remodeling effect in the model that we call MCF remodeling. In accordance with the experiments, the AF impairs the force of contraction [9, 10] and rates of activation and relaxation [11], and the sensitivity of the thin filament [11]. Accordingly, we increased the activation of TRPN and reduced the cross bridge cycling (XBcy) rates. However, the percentage level of change and the mechanisms behind have not been described in detail. Therefore, in the mechanical part of the model, we made a manual tunning of parameters i.e. the unbinding rate of the regulatory unit (RU) k_{off}, disassociation coefficient k_d, XBcy transition rate k_{basic}, and the factor of apparent cooperativity (γ). This tunning of parameters was aided by the experimental data obtained by our literature study. Hence, we made a sensitivity analysis for each parameter change and ended up with a level of change that is more inline with the experimental data and is listed in Table 1. After this, the last effect included the SERCA uptake remodeling (shown in Table 1) that was achieved by the loss of SERCA pumping function [12, 13].

Using the cAF remodeled version of MBS2022, we quantified the characteristics of the model output in comparison to the control model output. For this, we collected biomarkers related to AP, CaT, and force of contraction (F_{active}) defined in Table 2. All these biomarkers are computed as difference δ between cAF and sinus rhythm experimental values obtained from the references as shown in Table 2.

3. Results

The effect of AF induced remodeling on MBS2022 model has been shown in Figure 1. The control model output (in blue solid line) is compared with cAF output by incorporating electrical (in red dashed line), CaMKII (in yellow dot-dashed line), MCF (in blue dashed line), and SERCA (in black dotted line) remodeling effect. The AF induced AP is quite triangular in shape with a prominent plateau and has a short APD with a hyperpolarized V_{diast} in comparison with the control model as shown in Figure 1A. No difference is observed in cAF AP shape by the incorporation of other remodeling effects.

Electrical remodeling has shown a major drop in both systolic and diastolic CaT for both compartments (Figure 1B&C in red dashed line). This reduction of CaT_{peak} in the cytosol is because of the Ca^{2+}-handling remodeling i.e., reduced Ca^{2+}-release from the SR, and enhanced SR-Ca leak with no effect on SERCA uptake. As a result, the electrical remodeling results in almost 80% reduction in SR-Ca content in both compartments as shown in Figure 1D&E. Consequently, a 66% reduction in F_{active} systolic and diastolic values is observed (Figure 1F). A quantitative comparison of AP, CaT, and F_{active} biomarkers is shown in Table 2 where an increase in diastolic levels for both CaT and F_{active} under cAF can be seen.

Remodeling of CaMKII effect results in 16% rise in

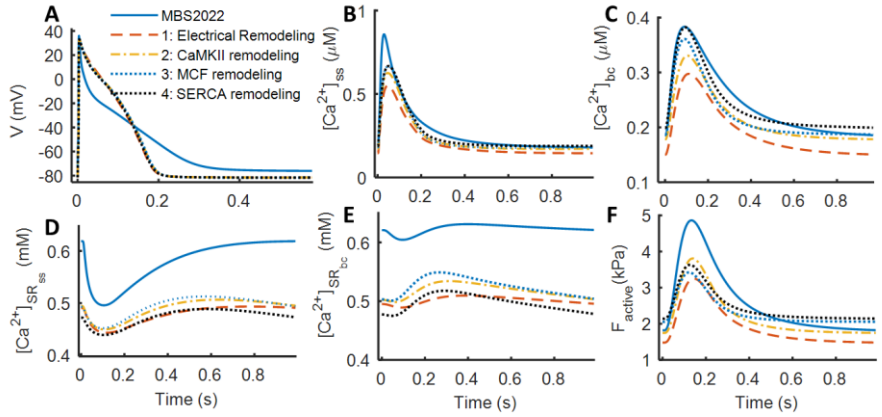

Figure 1: Atrial Fibrillation remodeling effect incorporated in MBS2022 model in an incremental way. The control model (in blue solid line), starting with electrical remodeling effect (in red dashed line), then included CaMKII remodeling (in yellow dot dashed line), addition of MCF remodeling (in blue dotted line), and at the end is the SERCA remodeling effect (in black dotted line) has been compared. A) shows the shortening of action potential (AP) under cAF condition, CaT in the *ss* B) and *bc* C) compartments, Ca^{2+}-SR contents in *ss* D) and *bc* E) compartments, and F) the force of contraction F_{active}.

diastolic CaT in both compartments (Figure 1B&C). However, this rise results in a diastolic value that is still less than the control (Figure 1C). On the same lines, the F_{active} diastole is still less than the control value hence, that contradicts the experimental trend (as reported in Table 2). Impaired MCF machinery raised the CaT amplitude in the *bc* (Figure 1C) since less Ca^{2+} is bound to the TRPN buffer resulting in depressed contraction with a raised relaxation value (Figure 1F). The addition of SERCA remodeling effect results in the rise in diastolic value for both CaT (Figure 1C) and F_{active} (Figure 1F) as compared to control condition. Depression of SERCA activity has reduced the SR-Ca^{2+} load the most, in particular, for the *bc* compartment (Figure 1E).

Table 2: Comparison of cAF remodeling response on MBS2022 model with experimental data references. Experimental data references were used to calibrate and compare the cAF model output. Biomarkers shown are difference between cAF and SR (δ) values for action potential duration at 90% of repolarization (APD_{90}), plateau potential (PLT_{20}) defined as the mean absolute potential in the window of 20% and 30% of APD_{90}, amplitude (V_{amp}), diastolic potential (V_{diast}), maximal shortening velocity (dV/dt_{max}). For CaT, difference of CaT amplitude (Ca_{amp}), its diastolic value (Ca_{diast}), decay time (CaTτ), caffeine induced CaT decay time (cCaTτ) has been shown. Similarly, for force F_{active}, biomarkers are the amplitude ($F_{active\ amp}$), the diastolic value ($F_{active\ diast}$), and the relaxation time at 90% of time (rt_{90}).

Biomarker δ=cAF-SR	**References**	**Experimental data**	**Model output**
δAPD_{90} (ms)	Bosch 1999, Wagoner 1999, Dobrev 2003, Wettwer 2004, Ford 2016, Schotten 2002	-36, -170	-73
δPLT_{20} (mV)		14.7	26.1
δV_{amp} (mV)	Ford 2016	7.1	2.3
$\delta dV/dt_{max}$ (mV/ms)		43.5	4.9
δV_{diast} (mV)	Ford 2016, Wettwer 2004	-2.4, -5	-5.4
δCaT_{amp} (nM)	Voigt 2012	-100	-38
δCaT_{diast} (nM)	Voigt 2012, Neef 2010	45, 70	12
δCaTτ (ms)	Voigt 2012	80	-14
δcCaTτ (ms)		-800	-441.3
$\delta F_{active\ amp}$ (kPa)	Schotten 2002, Schotten 2006, Sossalla 2010, Schwinger 1993	-1.72, -7.60	-3.21
$\delta F_{active\ diast}$ (kPa)	Sossalla 2010	0.6	0.33
$\delta rt_{90Factive}$ (ms)	Schotten 2002	14	-102

Biomarkers shown in Table 2 demonstrate the model output incorporated with overall remodeling effects. The model output is compared with the experimental data either in the form of absolute difference or as a range of differences where the sign represents increasing or decreasing trend under cAF condition. Under cAF condition, APD_{90} is shortened, PLT_{20} and dV/dt_{max} have been increased, and V_{diast} has been hyperpolarized following the data trend. For the CaT, the CaT_{amp} has been dropped, with raised CaT_{diast}, and cCaTτ has been lengthened in line with the experimental data whereas, CaTτ is showing a slight lengthening effect in contrast to the data reported. The biomarkers for F_{active} demonstrated a depressed $F_{active\ amp}$ with elevated $F_{active\ diast}$ following the experimental data; however, the $rt_{90Factive}$ is showing a contradictory lengthening effect.

Based on the calibrated set of parameters (from Table 2) for cAF, we have extended the analysis for rate adaptation of AP and CaT/F_{active} as shown in Figure 2 and 3 respectively. The rate of shortening of APD_{90} with varying rates is more pronounced in SR (in blue) than cAF (in red) (as shown in Figure 2C) that qualitatively meets with the data shown by Ford et al. [14].

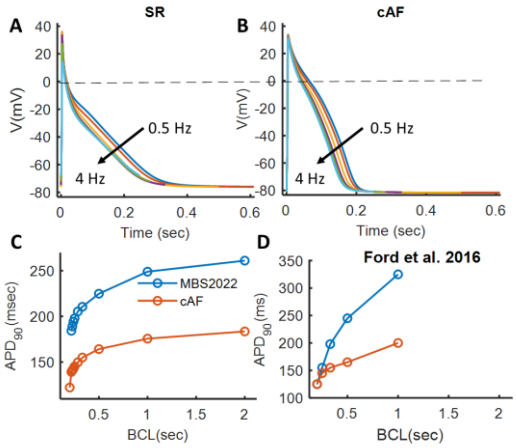

Figure 2: A & B) Comparison of APs for SR and cAF versions under varying BCL from 2sec to 0.25sec; C & D) show comparison of APD_{90} trend in SR vs cAF with experimental data from [14].

The elevation of CaT and F_{active} with rate is shown in Figure 3. The percentage rise has been increased in cAF condition for CaT (Figure 3B). The dome-shaped trend of %δ F_{active} with rate is lost for cAF condition that qualitatively meets with the experimental trend (Figure 3C bottom) [15] where the biphasic decrease is shifted to higher frequency. The $\%\delta CaT_{peak}$ and $\%\delta CaT_{diast}$ trend with rate is again more enhanced in cAF condition than control model.

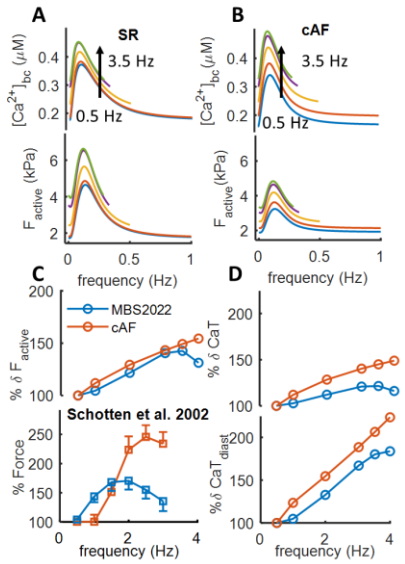

Figure 3: CaT (top) and F_{active} (bottom) traces for varying rates from 0.5Hz to 3.5Hz in SR (A) and cAF (B) conditions. The biomarkers trend C) $\%\delta F_{active\ peak}$ for model output (top) vs data [15] (bottom), and D) $\%\delta CaT_{peak}$ (top) and $\%\delta CaT_{diast}$ (bottom).

4. Discussion & Conclusions

We have presented cAF version of our recently developed EM coupled model. For cAF, the model has demonstrated a triangular AP with short APD_{90} and hyperpolarized V_{diast} inline with many studies as already seen by references listed in Table 2. The CaT and F_{active} demonstrated a depression in amplitude and elevation of diastolic level vs control. For amplitude reduction, downregulation of g_{CaL} and increased extrusion of Ca^{2+} from the cytosol via NaCa exchanger are responsible for this impairment as was previously observed by Schotten et al. [15, 9]. Inline with this experimental result, our model demonstrates a maximum depression of CaT and F_{active} amplitude for electrical remodeling (Figure 1C&F).

The raised CaT_{diast} levels are associated with the development of a potential arrhythmogenic substrate that could trigger or maintain AF as was analyzed in studies by Neef et al. [7], and Voigt et al. [13] though the underlying mechanisms were variable among both studies. The common mechanism was the increased CaMKII-dependent phosphorylation of RyRs leading to enhanced SR-Ca^{2+} leak however, Voigt et al. reported a larger I_{NaCa} as another factor responsible for a given SR-Ca^{2+} release. In our model, CaMKII remodeling effect enhanced the diastolic level of CaT but not more than control level (as was reported in Table 2). Since,the diastolic level of CaT_{bc} is dependent on SERCA activity hence, we depressed the SERCA uptake and found a prominent elevation of CaT_{diast}. This is in accordance to the experimental results, where the hyperphosphorylation of inhibitory protein phospholamban resulted in loss-of-function of SERCA activity [12].

References

[1] Hindricks G, et al. 2020 ESC Guidelines for the diagnosis and management of AF developed in collaboration with the European Association for Cardio-Thoracic Surgery (EACTS), ESC Scientific Document Group, European heart journal. 2021 Feb 1;42(5):373-498.

[2] Heijman J, Dobrev D. Determinants and therapeutic potential of calcium handling abnormalities in AF: what can we learn from computer models?, JP. 2022 Oct 8.

[3] Heijman J, et al. Computational models of AF: Achievements, challenges, and perspectives for improving clinical care. CVR, 2021 Jun 15;117(7):1682-99.

[4] Mazhar F, et al. A Detailed Mathematical Model of the Human Atrial Cardiomyocyte: Integration of Electrophysiology and Cardiomechanics" Under Revision in special issue 'Cardiac Mechano-Electric Crosstalk', JP.

[5] Grandi E, et al. Human atrial action potential and Ca^{2+} model: SR and cAF. Circ. Res. 2011 Oct 14;109(9):1055-66.

[6] Chang KC, et al. Disrupted calcium release as a mechanism for atrial alternans associated with human AF. PLoS Comp. Biol. 2014 Dec 11;10(12): e1004011.

[7] Neef S, et al. CaMKII-dependent diastolic SR Ca^{2+} leak and elevated diastolic Ca^{2+} levels in right atrial myocardium of patients with AF. Circ. Res. 2010 Apr 2;106(6):1134-44.

[8] Heijman J, et al. Calcium dysregulation in AF: the role of CaMKII. Frontiers in pharmacology. 2014 Mar 4;5:30.

[9] Schotten U, et al. Cellular mechanisms of depressed atrial contractility in patients with cAF. Circulation. 2001 Feb 6;103(5):691-8.

[10] Schotten U, et al. Blockade of atrial-specific K^{+}-currents increases atrial but not ventricular contractility by enhancing reverse mode Na^{+}/Ca^{2+}-exchange. CVR, 2007 Jan1;73(1):37-47.

[11] Belus A, et al. Effects of cAF on active and passive force generation in human atrial myofibrils. Circ. Res. 2010 Jul 9;107(1):144-52.

[12] El-Armouche A, et al. Molecular determinants of altered Ca^{2+} handling in human cAF. Circulation. 2006 Aug 15;114(7):670-80.

[13] Voigt N, et al. Enhanced SR Ca^{2+} leak and increased Na^{+}-Ca^{2+} exchanger function underlie delayed afterdepolarizations in patients with cAF. Circulation. 2012 May 1;125(17):2059-70.

[14] Ford J, et al. The positive frequency-dependent electrophysiological effects of the IKur inhibitor XEN-D0103 are desirable for the treatment of AF. Heart Rhythm. 2016 Feb 1;13(2):555-64.

[15] Schotten U, et al. AF-induced atrial contractile dysfunction: a tachycardiomyopathy of a different sort. CVR. 2002 Jan 1;53(1):192-201.

Address for correspondence:
Stefano Severi
Department of Electrical, Electronic and Information Engineering, University of Bologna,
Via dell'Università 50, 47522 Cesena (FC), Italy
stefano.severi@unibo.it